

# Quantum theory of light emission from a semiconductor quantum dot

T. Feldtmann,\* L. Schneebeli, M. Kira, and S. W. Koch

*Department of Physics and Materials Sciences Center, Philipps-University Marburg, Renthof 5, 35032 Marburg, Germany*

(Received 5 December 2005; revised manuscript received 17 February 2006; published 18 April 2006)

A fully quantum-mechanical theory for the spontaneous light emission from the interacting electron-hole system in a quantum dot is developed. Using a cluster-expansion approach, a closed set of equations of motion for singlets and two-particle correlations is derived. Photoluminescence spectra are calculated and the radiative decay dynamics is discussed.

DOI: [10.1103/PhysRevB.73.155319](https://doi.org/10.1103/PhysRevB.73.155319)

PACS number(s): 78.67.Hc, 42.50.Ct, 73.21.La

## I. INTRODUCTION

A number of recent experiments<sup>1–6</sup> has demonstrated that isolated semiconductor quantum dots are capable of emitting nonclassical light. Already for continuous-wave excitation, photon-antibunching effects can lead to sub-Poissonian emission statistics,<sup>5</sup> while in case of a pulsed excitation, emission of a single photon<sup>2–4</sup> or one pair of strongly correlated photons<sup>6</sup> per each excitation pulse has been observed. This truly quantum-mechanical behavior opens the door to future applications of quantum dots in quantum cryptography<sup>7</sup> as well as quantum computing<sup>8,9</sup> and data storing.<sup>10</sup>

Already the theoretical description of the quantum-dot carrier system is a sophisticated many-body problem.<sup>11–22</sup> As a general tendency, the three-dimensional confinement strongly enhances the Coulomb correlations between the dot electrons and holes. To investigate the properties of these correlations and their effect on the optical resonances of the system, both partial and full diagonalization techniques<sup>11–18</sup> as well as configuration-interaction calculations<sup>19–21</sup> have been applied.

The methods above can successfully solve the specific details of an isolated dot; one can accurately describe, e.g., emission and absorption lines. However, this approach becomes rather involved for a realistic quantum dot that is an open system due to interaction with a quantized multimode light field, wetting layer states,<sup>23</sup> and phonons.<sup>24</sup> Such coupling effects are often very dynamical, and they have successfully been described<sup>25–27</sup> in quantum-well systems using the cluster-expansion approach. In particular, we analyze the nonclassical emission from a quantum dot, which requires quantization of the light field. Therefore, we extend earlier theoretical approaches and present a fully quantum-mechanical theory for the spontaneous emission from the Coulomb interacting carrier system in a quantum dot. While we concentrate here on the internal electronic interaction, the theory we introduce has the potential to treat consistently different phenomena related to open quantum-dot systems.

We employ the equation-of-motion approach for the relevant correlation functions and systematically treat the resulting hierarchy problem by using the cluster-expansion technique. In Sec. II, we introduce the model Hamiltonian where the material part agrees with Refs. 15 and 18 while the light-matter interaction is described quantum electrodynamically. After a short summary of the main features of the cluster expansion in our system in Sec. III, we derive the

semiconductor Bloch equations (SBEs) for the quantum dot in Sec. IV. The SBEs describe the excitation of the carrier system when it is driven by a coherent light field.<sup>28</sup> In Sec. V, we then analyze the emission from the dot under incoherent conditions, which is described by the semiconductor luminescence equations (SLEs). We introduce an exciton basis that enables us to formulate analytic approximations for both the linear absorption and the stationary luminescence spectrum. In Sec. VI, we present a phenomenological description of a generic excitation process, and determine the physically allowed stable states of the dot in the incoherent regime. Finally, in Sec. VII, we calculate the luminescence from several of these stable states and identify plasma and excitonic contributions on the basis of their decay dynamics.

## II. MODEL HAMILTONIAN

The coupling of a quantum dot to a light field can be treated fully quantum mechanically by starting from the general system Hamiltonian<sup>29,30</sup>

$$H = H_{0,\text{ele}} + H_{0,\text{light}} + H_C + H_D \quad (1)$$

which contains contributions  $H_{0,\text{ele}}$  and  $H_{0,\text{light}}$  due to noninteracting electrons and light, respectively. The many-body and the quantum-optical dynamics follow from the Coulomb part of the Hamiltonian  $H_C$  and the light-matter part  $H_D$ . Expanding the electron states in the usual Bloch basis and using the envelope function approximation,<sup>31,32</sup> the pure carrier Hamiltonian (1) can be written as

$$H_{0,\text{ele}} = \sum_{\lambda\beta} E_{\beta}^{\lambda} a_{\lambda\beta}^{\dagger} a_{\lambda\beta}, \quad (2)$$

$$H_C = \frac{1}{2} \sum_{\lambda\lambda'} \sum_{\beta_1, \dots, \beta_4} V_{\beta_3\beta_4}^{\beta_1\beta_2} a_{\lambda\beta_1}^{\dagger} a_{\lambda'\beta_2}^{\dagger} a_{\lambda'\beta_3} a_{\lambda\beta_4} \quad (3)$$

where  $\lambda$  labels the band index of the Bloch electrons while  $\beta$  identifies the quantum numbers of the envelope part. When the electrons are confined to a lens-shaped dot on a planar wetting layer (i.e., quantum well), its envelope function can accurately be described via the harmonic oscillator wave functions confined in two directions.<sup>33</sup> Thus, the envelope part is defined by  $\beta = (n, m, \sigma)$  with the principal quantum number  $n = 0, 1, 2, \dots$ , the angular-momentum quantum num-

ber  $m = -n, -n+2, \dots, n-2, n$ , and the spin  $\sigma$ . The fermionic operators  $a_{\lambda\beta}^\dagger$  and  $a_{\lambda\beta}$  create and annihilate, respectively, a Bloch electron in band  $\lambda$  with envelope function  $\zeta_\beta(\mathbf{r})$  as calculated in Appendix A.

In this paper, we restrict the analysis to a two-band model with a single valence band  $\lambda=v$  and a single conduction band  $\lambda=c$ . In this case, the single-particle energies simply follow from

$$E_\beta^c \equiv E_\beta^e = n\hbar\omega_e + E_g, \quad (4)$$

$$E_\beta^v \equiv -E_\beta^h = -n\hbar\omega_h, \quad (5)$$

where  $E_g$  is the band-gap energy. In Appendix B, it is shown that the Coulomb matrix elements are real valued and obey the selection rules

$$V_{\beta_3\beta_4}^{\beta_1\beta_2} = \delta_{m_1+m_2, m_3+m_4} \delta_{\sigma_1, \sigma_4} \delta_{\sigma_2, \sigma_3} V_{\beta_3\beta_4}^{\beta_1\beta_2}. \quad (6)$$

Also the following symmetries:

$$V_{\beta_3\beta_4}^{\beta_1\beta_2} = V_{\beta_1\beta_2}^{\beta_3\beta_4}, \quad (7)$$

$$V_{\beta_3\beta_4}^{\beta_1\beta_2} = V_{\beta_4\beta_3}^{\beta_2\beta_1} \quad (8)$$

are generally valid.

For a quantum-electrodynamical treatment of the light-matter interaction,<sup>29,30</sup> we start from the quantized transverse electric field

$$\mathbf{E}(\mathbf{r}) = \sum_{\mathbf{q}\alpha} \mathcal{E}_q [iU_{\mathbf{q}\alpha}(\mathbf{r})B_{\mathbf{q}\alpha}(t) + \text{H.c.}] \hat{\mathbf{e}}_\alpha, \quad (9)$$

where  $\mathbf{q}$  denotes the wave vector and  $\hat{\mathbf{e}}_\alpha$  ( $\alpha=1,2$ ) defines the polarization direction of the eigenmode  $U_{\mathbf{q}\alpha}$ . In the following, we suppress the index  $\alpha$  for notational simplicity. The photon operators  $B_{\mathbf{q}}, B_{\mathbf{q}}^\dagger$  satisfy bosonic commutation relations. Moreover, we have introduced the vacuum-field amplitude  $\mathcal{E}_q \equiv \sqrt{\hbar\omega_q/(2\epsilon_0)}$ . As a result of quantization, the light field has

$$H_{0,\text{light}} = \sum_{\mathbf{q}} \hbar\omega_q \left( B_{\mathbf{q}}^\dagger B_{\mathbf{q}} + \frac{1}{2} \right) \quad (10)$$

with the dispersion relation  $\omega_q = c_0|\mathbf{q}|$ , where  $c_0$  denotes the vacuum velocity of light.

When the quantum dot is positioned at  $\mathbf{r}=\mathbf{0}$ , the dipole-interaction Hamiltonian leads to

$$H_D = \sum_{\beta\mathbf{q}} [i(\mathcal{F}_{\mathbf{q}}^* B_{\mathbf{q}}^\dagger - \mathcal{F}_{\mathbf{q}} B_{\mathbf{q}}) a_{v\beta}^\dagger a_{c\beta} + \text{H.c.}] \quad (11)$$

where the coupling constant

$$\mathcal{F}_{\mathbf{q}} \equiv \mathcal{E}_q U_{\mathbf{q}}(\mathbf{0}) \hat{\mathbf{e}}_\alpha \cdot \mathbf{d}_{vc} \quad (12)$$

contains the dipole matrix element  $\mathbf{d}_{vc}$ .

For all numerical examples in this paper, we choose material parameters that are typical for self-assembled indium-based quantum dots. We assume effective electron and hole masses  $m_e = 0.065m_0$  and  $m_h = 0.170m_0$ , respectively. The quantum-well confinement is characterized by a confinement width of  $L = 40 \text{ \AA}$  [see Appendix A, Eq. (A2)] while for

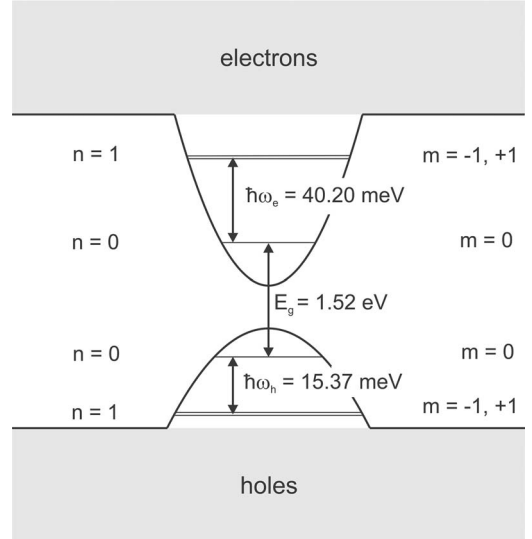


FIG. 1. Energy levels of the quantum dot. The shaded areas indicate the wetting-layer continuum.

the in-plane confinement, we take  $\hbar\omega_e = 40.20 \text{ meV}$  and  $\hbar\omega_h = 15.37 \text{ meV}$ . In Ref. 33, it is discussed in detail how these confinement parameters depend on the geometry of the dot. To fully determine the material Hamiltonian, we assume the band-gap energy  $E_g = 1.52 \text{ eV}$  and the dielectric constant  $\epsilon = 13.69$ .

The parabolic confinement potentials are truncated by dissociation thresholds. Consequently, for principal quantum numbers  $n$  higher than a certain  $n_{\text{max}}$ , the envelope functions do not correspond to dot states any longer, and their energies are hidden in the quasicontinuum of the wetting-layer states. While all equations will be derived for the most general case, we restrict their explicit evaluation in this paper to  $n_{\text{max}} = 1$ , i.e., to a quantum dot that contains only  $s$  and  $p$  shells for both electrons and holes. Moreover, we investigate the spin-selective case where only one of the spin species is considered such that the dot states are determined by  $n$  and  $m$  alone. Figure 1 schematically displays the energy levels of the material system.

### III. CLUSTER EXPANSION

In general, all relevant operators can be classified by determining how many fermion or boson operators they contain. The class of  $N$ -particle operators is given by

$$O_N = a_{i_N}^\dagger \cdots a_{i_1}^\dagger a_{i_1} \cdots a_{i_N}, \quad (13)$$

where photon operators formally correspond to pairs of carrier operators  $B_{\mathbf{q}} \sim a_{\mathbf{q}}^\dagger a_{\mathbf{q}}$ . The Heisenberg equations of motion  $i\hbar\partial_t O = [O, H]$  have the structure

$$\frac{\partial}{\partial t} O_N = T[O_N] + V[O_{N+1}], \quad (14)$$

where the functional  $T$  mainly results from the noninteracting part  $H_0 = H_{0,\text{ele}} + H_{0,\text{light}}$  of the Hamiltonian while the functional  $V$  originates from the interacting part  $H_C + H_D$ ,

respectively. Hence,  $N$ -particle operators are coupled to  $(N+1)$ -particle operators via  $V$ , which leads to the well-known hierarchy problem of many-body physics.<sup>32,34</sup>

One successful approach to deal with the hierarchy problem is provided by the so-called *cluster expansion*.<sup>25,35–38</sup> Here, one factorizes  $N$ -particle expectation values in terms of independent single particles (singlets), correlated pairs (doublets), correlated three-particle clusters (triplets), and so on, up to correlated  $N$ -particle clusters. The hierarchy problem can then be treated consistently by truncating the right-hand side of Eq. (14) such that one includes all clusters up to a desired order.

In practice, the cluster expansion is performed according to the recursion scheme

$$\langle O_2 \rangle = \langle O_2 \rangle_S + \Delta \langle O_2 \rangle, \quad (15)$$

$$\begin{aligned} \langle O_3 \rangle &= \langle O_3 \rangle_S + \langle O_1 \rangle \Delta \langle O_2 \rangle + \Delta \langle O_3 \rangle, \\ &\vdots \end{aligned} \quad (16)$$

$$\begin{aligned} \langle O_N \rangle &= \langle O_N \rangle_S + \langle O_{N-2} \rangle_S \Delta \langle O_2 \rangle + \langle O_{N-4} \rangle_S \Delta \langle O_2 \rangle \Delta \langle O_2 \rangle + \dots \\ &\quad + \Delta \langle O_N \rangle, \end{aligned} \quad (17)$$

where  $\Delta \langle O_N \rangle$  denotes the purely correlated part of the  $N$ -particle cluster. Each term on the right-hand side of Eq. (17) represents the fully antisymmetrized (for fermionic operators) or symmetrized (for bosonic operators) sum over all possibilities to distribute the  $N$  creation and  $N$  annihilation operators among the different clusters. As a starting point of the recursion scheme,  $\langle O_N \rangle_S$  leads to the Hartree-Fock factorization for the carrier operators while the singlet part for the photon operators produces the classical factorization for the light field. For our purposes, it will be sufficient to truncate the hierarchy of equations on the doublet level.

#### IV. SEMICONDUCTOR BLOCH EQUATIONS

The proper two-point quantities can be distinguished into polarization expectation values

$$p_{\beta'}^\beta \equiv \langle a_{v\beta}^\dagger a_{c\beta'} \rangle, \quad (18)$$

and density expectation values

$$f_{e\beta'}^\beta \equiv \langle a_{c\beta}^\dagger a_{c\beta'} \rangle, \quad (19)$$

$$f_{h\beta'}^\beta \equiv \delta_{\beta\beta'} - \langle a_{v\beta}^\dagger a_{v\beta'} \rangle. \quad (20)$$

Their coupled equations of motion form the *semiconductor Bloch equations*

$$\begin{aligned} i\hbar \frac{\partial}{\partial t} p_{\beta'}^\beta &= \sum_{\beta_1} (E_{\beta'\beta_1}^e p_{\beta_1}^\beta + E_{\beta_1\beta}^h p_{\beta'}^{\beta_1}) - \mathbf{d}_{cv} \langle \mathbf{E} \rangle \\ &\quad \times (\delta_{\beta\beta'} - f_{h\beta'}^\beta - f_{e\beta'}^\beta) - \sum_{\beta_1\beta_2\beta_3\beta_4} V_{\beta_1\beta_4}^{\beta_2\beta_3} \\ &\quad \times (\delta_{\beta\beta_1} \delta_{\beta_2\beta'} - \delta_{\beta\beta_1} f_{e\beta'}^{\beta_2} - \delta_{\beta_2\beta'} f_{h\beta_1}^\beta) p_{\beta_4}^{\beta_3} + D_{p\beta'}^\beta, \end{aligned} \quad (21)$$

$$\begin{aligned} i\hbar \frac{\partial}{\partial t} f_{e\beta'}^\beta &= \sum_{\beta_1} (E_{\beta'\beta_1}^e f_{e\beta_1}^\beta - E_{\beta_1\beta}^e f_{e\beta'}^{\beta_1}) + \mathbf{d}_{cv} \langle \mathbf{E} \rangle p_{\beta'}^\beta \\ &\quad - [\mathbf{d}_{cv} \langle \mathbf{E} \rangle p_{\beta'}^{\beta'}]^* - \sum_{\beta_1\beta_2\beta_3} [V_{\beta_1\beta_3}^{\beta'\beta_2} p_{\beta_3}^{\beta_2} (p_{\beta'}^{\beta_1})^* \\ &\quad - V_{\beta_1\beta_3}^{\beta\beta_2} (p_{\beta_3}^{\beta_2})^* p_{\beta'}^{\beta_1}] + D_{e\beta'}^\beta, \end{aligned} \quad (22)$$

$$\begin{aligned} i\hbar \frac{\partial}{\partial t} f_{h\beta'}^\beta &= - \sum_{\beta_1} (E_{\beta'\beta_1}^h f_{h\beta_1}^\beta - E_{\beta_1\beta}^h f_{h\beta'}^{\beta_1}) + \mathbf{d}_{cv} \langle \mathbf{E} \rangle p_{\beta'}^\beta \\ &\quad - [\mathbf{d}_{cv} \langle \mathbf{E} \rangle p_{\beta'}^{\beta'}]^* + \sum_{\beta_1\beta_2\beta_3} [V_{\beta_1\beta_3}^{\beta_1\beta_2} (p_{\beta_3}^{\beta_2})^* p_{\beta_1}^\beta \\ &\quad - V_{\beta_1\beta_3}^{\beta_1\beta_2} p_{\beta_3}^{\beta_2} (p_{\beta_1}^{\beta'})^*] + D_{h\beta'}^\beta. \end{aligned} \quad (23)$$

In Eqs. (21)–(23) the first lines always contain the mean-field energies

$$E_{\beta\beta'}^e \equiv \delta_{\beta\beta'} E_\beta^e - \sum_{\beta_1\beta_2} V_{\beta'\beta_2}^{\beta\beta_1} f_{e\beta_2}^{\beta_1} + \sum_{\beta_1\beta_2} V_{\beta_2\beta'}^{\beta\beta_1} (f_{e\beta_2}^{\beta_1} - f_{h\beta_2}^{\beta_1}), \quad (24)$$

$$E_{\beta\beta'}^h \equiv \delta_{\beta\beta'} E_\beta^h - \sum_{\beta_1\beta_2} V_{\beta'\beta_2}^{\beta\beta_1} f_{h\beta_2}^{\beta_1} - \sum_{\beta_1\beta_2} V_{\beta_2\beta'}^{\beta\beta_1} (f_{e\beta_2}^{\beta_1} - f_{h\beta_2}^{\beta_1}). \quad (25)$$

Formally,  $E_{\beta\beta'}^{e(h)}$  also includes terms such as  $U_{\beta'}^\beta \equiv \sum_{\beta_1} V_{\beta'\beta_1}^{\beta\beta_1}$  which lead to a divergence since the summation over  $\beta_1$  runs over all states of the system including the extended wetting-layer states. However, the completeness relation of the envelope functions and the explicit form of  $V_{\beta'\beta_1}^{\beta\beta_1}$  [see Eq. (B4)] provide  $U_{\beta'}^\beta = \delta_{\beta\beta'} U$  where  $U$  does not depend on  $\beta$ . Thus, these formally infinite terms are already included in the band-gap energy such that they do not appear in Eqs. (24) and (25).

The second lines of Eqs. (21)–(23) contain the classical electric field  $\langle \mathbf{E} \rangle$  which drives the polarization and thus contributes to the creation of electron and hole densities. Often,  $\mathbf{d}_{cv} \langle \mathbf{E} \rangle$  is referred to as the Rabi frequency, and its Coulomb renormalizations are found in the third lines of Eqs. (21)–(23). For a quantum-dot system, these renormalizations are somewhat more complicated than the corresponding terms for quantum wells.<sup>30</sup>

We see from the SBEs that the singlet dynamics couples to pure doublet terms indicated by  $D_{p\beta'}^\beta$ ,  $D_{e\beta'}^\beta$ , and  $D_{h\beta'}^\beta$ . They originate from Coulombic and quantum-optical correlations. Explicitly, these terms can be written as

$$\begin{aligned} D_{p\beta'}^\beta &= - \sum_{\beta_1\beta_2\beta_3} \left[ V_{\beta_2\beta_3}^{\beta'\beta_1} \sum_{\lambda} C \left( \begin{array}{c} v\lambda \\ \lambda c \end{array} \middle| \begin{array}{c} \beta\beta_1 \\ \beta_2\beta_3 \end{array} \right) \right. \\ &\quad \left. - V_{\beta_2\beta_3}^{\beta\beta_1} \sum_{\lambda} C \left( \begin{array}{c} v\lambda \\ \lambda c \end{array} \middle| \begin{array}{c} \beta_3\beta_2 \\ \beta_1\beta' \end{array} \right) \right] + i(\Delta \langle B_{\Sigma} a_{c\beta}^\dagger a_{c\beta'} \rangle \\ &\quad - \Delta \langle B_{\Sigma} a_{v\beta}^\dagger a_{v\beta'} \rangle), \end{aligned} \quad (26)$$

$$\begin{aligned}
 D_{e\beta'}^\beta = & - \sum_{\beta_1\beta_2\beta_3} \left[ V_{\beta_2\beta_3}^{\beta'\beta_1} \sum_{\lambda} C \left( \begin{matrix} c\lambda \\ \lambda c \end{matrix} \middle| \begin{matrix} \beta\beta_1 \\ \beta_2\beta_3 \end{matrix} \right) \right. \\
 & \left. - V_{\beta_2\beta_3}^{\beta\beta_1} \sum_{\lambda} C \left( \begin{matrix} c\lambda \\ \lambda c \end{matrix} \middle| \begin{matrix} \beta_3\beta_2 \\ \beta_1\beta' \end{matrix} \right) \right] + i(\Delta \langle B_{\Sigma}^{\dagger} a_{v\beta}^{\dagger} a_{c\beta'} \rangle \\
 & + \Delta \langle B_{\Sigma}^{\dagger} a_{v\beta'}^{\dagger} a_{c\beta} \rangle^*), \quad (27)
 \end{aligned}$$

$$\begin{aligned}
 D_{h\beta'}^\beta = & \sum_{\beta_1\beta_2\beta_3} \left[ V_{\beta_2\beta_3}^{\beta'\beta_1} \sum_{\lambda} C \left( \begin{matrix} \lambda v \\ v\lambda \end{matrix} \middle| \begin{matrix} \beta_1\beta \\ \beta_3\beta_2 \end{matrix} \right) \right. \\
 & \left. - V_{\beta_2\beta_3}^{\beta\beta_1} \sum_{\lambda} C \left( \begin{matrix} \lambda v \\ v\lambda \end{matrix} \middle| \begin{matrix} \beta_2\beta_3 \\ \beta'\beta_1 \end{matrix} \right) \right] + i(\Delta \langle B_{\Sigma}^{\dagger} a_{v\beta}^{\dagger} a_{c\beta'} \rangle \\
 & + \Delta \langle B_{\Sigma}^{\dagger} a_{v\beta'}^{\dagger} a_{c\beta} \rangle^*), \quad (28)
 \end{aligned}$$

where we have identified the genuine two-particle correlations

$$C \left( \begin{matrix} \lambda\lambda' \\ \lambda''\lambda''' \end{matrix} \middle| \begin{matrix} \beta\beta' \\ \beta''\beta''' \end{matrix} \right) \equiv \Delta \langle a_{\lambda\beta}^{\dagger} a_{\lambda'\beta'}^{\dagger} a_{\lambda''\beta''} a_{\lambda'''\beta'''} \rangle. \quad (29)$$

In our further derivations, we investigate the specific dynamics of excitonic electron-hole correlations

$$C_{x\beta''\beta'''}^{\beta\beta'} \equiv C \left( \begin{matrix} cv \\ vc \end{matrix} \middle| \begin{matrix} \beta\beta' \\ \beta''\beta''' \end{matrix} \right) \quad (30)$$

as well as electron-electron and hole-hole correlations

$$C_{e\beta''\beta'''}^{\beta\beta'} \equiv C \left( \begin{matrix} cc \\ cc \end{matrix} \middle| \begin{matrix} \beta\beta' \\ \beta''\beta''' \end{matrix} \right), \quad (31)$$

$$C_{h\beta''\beta'''}^{\beta\beta'} \equiv C \left( \begin{matrix} vv \\ vv \end{matrix} \middle| \begin{matrix} \beta\beta' \\ \beta''\beta''' \end{matrix} \right), \quad (32)$$

respectively. By using the rotating-wave approximation, the photon correlation terms can be expressed with the help of a collective photon operator

$$B_{\Sigma} \equiv \sum_{\mathbf{q}} \mathcal{F}_{\mathbf{q}} B_{\mathbf{q}}, \quad (33)$$

which basically describes the operator form of the Rabi frequency.

The two-particle correlations which include photon operators provide quantum-optical corrections to the SBEs. For example,  $D_e$  and  $D_h$  lead to spontaneous recombination of electron-hole pairs which is observed as reduction of carrier densities. The Coulomb correlations describe a variety of phenomena such as dephasing, energy renormalization, and scattering contributions.

If the system can be reduced to a closed set of dot states, one can diagonalize the Coulomb interaction with a given number of electrons and holes and determine the genuine many-body states and corresponding eigenenergies of the carrier system.<sup>18</sup> These states are stationary unless coupling to the light field or wetting layer is included. Since the cluster expansion describes the system exactly as long as the cluster number is larger than the particle number, two-particle correlations also provide terms that lead to the sta-

tionary states corresponding to the two-particle eigenstates. More specifically, such contributions are obtained from  $D_p$ ,  $D_e$ , and  $D_h$  terms that are limited to pure dot states. Since this feature is clearly present only for quantum-dot systems, we concentrate in this paper on resolving how the cluster expansion provides stationary states and characterize the quantum emission from the corresponding stationary states.

### A. Elliott formula for absorption

The precise inclusion of the two-particle correlations (26)–(28) is computationally rather demanding, especially, if the scattering from the wetting layer is fully included.<sup>23,39–41</sup> To gain some insight into coherent and classical excitation dynamics, we first simplify these contributions by including only their generic properties. The full singlet-doublet analysis is then performed later in Sec. V where the incoherent regime with quantum emission is investigated.

If we assume that the two-particle correlations  $D_p$ ,  $D_e$ , and  $D_h$  only lead to dephasing for the polarization when dot states are analyzed, we may replace  $D_{p\beta'}^\beta$  in Eq. (21) by a phenomenological dephasing term  $-i\gamma p_{\beta'}^\beta$ . If we further assume that the densities are quasistationary, Eqs. (22) and (23) can adiabatically be decoupled from Eq. (21). As a result, we find the frequency domain version of Eq. (21):

$$\begin{aligned}
 (\hbar\omega + i\gamma) p_{\beta'}^\beta(\omega) = & -d_{cv} \langle E \rangle(\omega) (\delta_{\beta\beta'} - f_{e\beta'}^\beta - f_{h\beta'}^\beta) \\
 & + \sum_{\beta_1\beta_2} A_{\beta\beta',\beta_1\beta_2} p_{\beta_2}^{\beta_1}(\omega), \quad (34)
 \end{aligned}$$

with the matrix  $\mathbf{A}$  defined by

$$\begin{aligned}
 A_{\beta\beta',\beta''\beta'''} \equiv & \delta_{\beta\beta'} E_{\beta''\beta'''}^e + \delta_{\beta'\beta''} E_{\beta''\beta'''}^h - \sum_{\beta_1\beta_2} V_{\beta_1\beta''}^{\beta_2\beta'} (\delta_{\beta\beta_1} \delta_{\beta_2\beta'} \\
 & - \delta_{\beta\beta_1} f_{e\beta'}^{\beta_2} - \delta_{\beta_2\beta'} f_{h\beta_1}^\beta). \quad (35)
 \end{aligned}$$

This matrix problem can be inverted such that  $p_{\beta'}^\beta$  can be expressed in terms of the exciting field. This result then yields the macroscopic polarization of the quantum dot,

$$\mathbf{P}(t) = \mathbf{d}_{cv} \sum_{\beta} \{ p_{\beta}^\beta(t) + [p_{\beta}^\beta(t)]^* \}, \quad (36)$$

as response to an external light field  $\langle \mathbf{E} \rangle$  which, for simplicity, we assume to be parallel to the dipole matrix element. The linear absorption spectrum then follows from

$$\alpha(\omega) \equiv \text{Im} \left[ \frac{P(\omega)}{\langle E \rangle(\omega)} \right], \quad (37)$$

which defines how the dot system absorbs a weak probe field.

By using the exciton basis introduced in Appendix C, one can diagonalize and invert Eq. (34). This procedure yields the *Elliott formula*<sup>42</sup>

$$\alpha(\omega) = |d_{vc}|^2 \text{Im} \left[ \sum_i \frac{\langle 1 | \phi^{i,R} \rangle \langle \phi^{i,L} | 1 - f_e - f_h \rangle}{\mathcal{E}_i - \hbar\omega - i\gamma} \right], \quad (38)$$

where  $|\phi^{i,R(L)}\rangle$  denotes the right- (left-)handed excitonic wave function with components  $\phi_{\beta\beta'}^{i,R(L)}$ , and



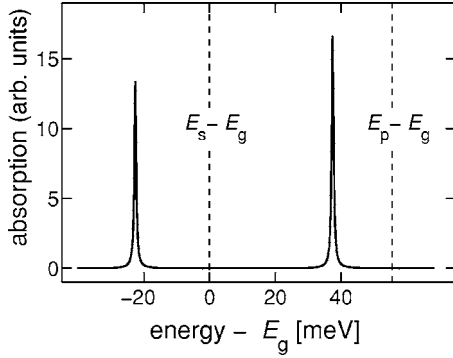


FIG. 2. Absorption spectrum for the unexcited dot. The excitonic resonances are positioned at  $\mathcal{E}_1 = E_g - 22.61$  meV and  $\mathcal{E}_2 = E_g + 37.50$  meV.  $E_s = E_g$  and  $E_p = E_g + 55.57$  meV mark the unrenormalized vertical transitions between the  $s$ - and the  $p$ -shell states, respectively.

$$\langle 1 | \phi^{i,R} \rangle = \sum_{\beta} \phi_{\beta\beta}^{i,R}, \quad (39)$$

$$\langle \phi^{i,L} | 1 - f_e - f_h \rangle = \sum_{\beta\beta'} (\phi_{\beta'\beta}^{i,L})^* (\delta_{\beta\beta'} - f_{e\beta\beta'}^{\beta} - f_{h\beta\beta'}^{\beta}). \quad (40)$$

The excitonic eigenenergies  $\mathcal{E}_i$  appearing in the denominator of the Elliott formula clearly define the spectral positions of the absorption resonances. When the Coulomb correlations are fully included in the analysis, they provide density-dependent energy renormalizations as well as excitation-induced dephasing<sup>39–41</sup> which also varies with the resonance index  $i$ . These effects are well known also from quasi-two-dimensional quantum-well structures.<sup>43,44</sup>

### B. Singlet properties of the system

The absorption spectrum for the unexcited dot is shown in Fig. 2. Out of the nine excitonic eigenstates only two are optically visible. In the following, we will refer to the low-energy resonance as the first, and to the high-energy resonance as the second exciton. In the absence of Coulomb interaction, the resonances coincide with the unrenormalized vertical transition energies  $E_s = E_g$  and  $E_p = E_g + \hbar(\omega_e + \omega_h)$ . Contrary to the quantum-well case, the second exciton absorption turns out to be even larger than the first one.

In Fig. 3(a), the excitonic eigenenergies are plotted as a function of the  $s$ -shell density for vanishing  $p$ -shell density. The energy  $\mathcal{E}_1$  of the first exciton features only a moderate shift, which means that no higher-order correlations are needed to obtain a spectrally stable position for the first resonance. Apparently, this result does not hold for the second excitonic energy  $\mathcal{E}_2$  that may well be influenced by higher-order clusters where also wetting-layer states have to be considered. We will therefore concentrate in this paper on configurations where the lowest exciton state is predominantly excited. In this case, the singlet-doublet analysis clearly provides sufficient accuracy.

Figure 3(b) shows the nonvanishing components of the first and the second right-handed excitonic wave functions. Again, a strong dependence on the  $s$ -shell density is only

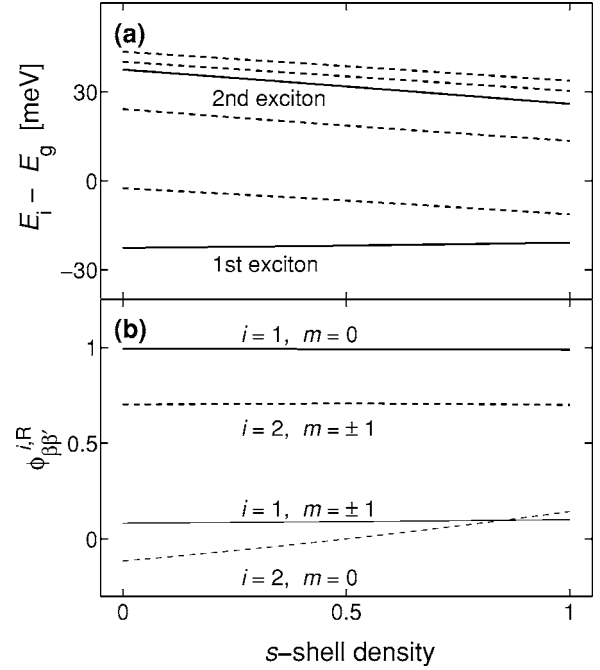


FIG. 3. (a) Dependence of the excitonic eigenenergies  $\mathcal{E}_i$  on the  $s$ -shell density for vanishing  $p$ -shell density. The solid lines refer to the optically visible excitons, the dashed lines to the dark excitons. The uppermost and the solid lines are nondegenerate; all other lines are twofold degenerate. (b) The nonvanishing components of the first and the second excitonic wave functions as function of the  $s$ -shell density. Additionally to the orthogonality relation between left- and right-handed exciton states [see Appendix C, Eq. (C3)], the right-handed wave functions have been normalized with respect to the Euclidean norm. Only the components  $\phi_{\beta\beta'}^{i,R}$  diagonal in  $\beta, \beta'$  are nonzero. They are unambiguously determined by the exciton label  $i$  and the angular momentum number  $m$ . Solid lines refer to  $i=1$ , dashed lines to  $i=2$ .

observed for the second exciton. From the two lines corresponding to the lowest exciton, one can clearly see that to a certain degree, the first exciton mixes  $s$ - and  $p$ -shell carrier states.

As a general result, pronounced excitonic effects turn out to be present even for high densities where the Pauli blocking becomes considerably strong. This feature clearly distinguishes the quantum dot from the 2D quantum-well case.<sup>26</sup> It is therefore interesting to investigate how electron-hole pairs become correlated or uncorrelated when the density is increased. While quantum-well excitons eventually become ionized,<sup>45</sup> quantum-dot excitons may still show large correlations even for elevated densities.

## V. SEMICONDUCTOR LUMINESCENCE EQUATIONS

The amount of relevant two-particle correlations reduces considerably as we investigate the entirely incoherent situation where the polarization  $p_{\beta\beta'}^{\beta}$  and the classical field  $\langle B_{\mathbf{q}} \rangle$  vanish for all  $\beta, \beta'$ , and  $\mathbf{q}$ . Since this regime also leads to interesting phenomena such as photoluminescence, we now analyze the quantum emission from stationary quantum-dot

states when the excitation levels become appreciable. When the system is incoherent, all singlets, except densities, remain zero during the evolution of the system. Furthermore, the quantum corrections and the Coulomb correlations in the equations of motion (22) and (23) for the densities become dominant once the coherent quantities disappear. Hence, it is crucial to consider the full set of equations of motion at the singlet-doublet level.

Under quasistationary conditions, the photoluminescence spectrum follows from the photon flux<sup>30</sup>

$$I_{\text{PL}}(\omega_{\mathbf{q}}) \equiv \frac{\partial}{\partial t} \langle B_{\mathbf{q}}^{\dagger} B_{\mathbf{q}} \rangle. \quad (41)$$

The equation of motion for the photon-number-like expectation values is given by

$$i\hbar \frac{\partial}{\partial t} \langle B_{\mathbf{q}}^{\dagger} B_{\mathbf{q}'} \rangle = \hbar(\omega_{\mathbf{q}'} - \omega_{\mathbf{q}}) \langle B_{\mathbf{q}}^{\dagger} B_{\mathbf{q}'} \rangle + i \sum_{\beta} \{ \mathcal{F}_{\mathbf{q}}^{\beta*} \Pi_{\beta}^{\beta}(\mathbf{q}) + \mathcal{F}_{\mathbf{q}} [\Pi_{\beta}^{\beta}(\mathbf{q}')]^* \}, \quad (42)$$

where we have defined the photon-assisted polarization

$$\Pi_{\beta'}^{\beta}(\mathbf{q}) \equiv \Delta \langle B_{\mathbf{q}}^{\dagger} a_{v\beta}^{\dagger} a_{c\beta'} \rangle \quad (43)$$

which contains the correlated part of the process where a photon is emitted via the recombination of an electron-hole pair.

The corresponding dynamics follows from

$$i\hbar \frac{\partial}{\partial t} \Pi_{\beta'}^{\beta}(\mathbf{q}) = -\hbar\omega_{\mathbf{q}} \Pi_{\beta'}^{\beta}(\mathbf{q}) + T_{\beta'}^{\beta}(\mathbf{q}) + \sum_{\beta_1\beta_2} A_{\beta\beta',\beta_1\beta_2} \Pi_{\beta_2}^{\beta_1}(\mathbf{q}) + iS_{\beta'}^{\beta}(\mathbf{q}) - i(\delta_{\beta\beta'} - f_{h\beta'}^{\beta} - f_{e\beta'}^{\beta}) \Delta \langle B_{\mathbf{q}}^{\dagger} B_{\Sigma} \rangle, \quad (44)$$

with the matrix  $\mathbf{A}$  as defined in Eq. (35). In the following, we will approximate the full three-particle scattering term  $T_{\beta'}^{\beta}(\mathbf{q})$  by a phenomenological dephasing term  $-i\gamma \Pi_{\beta'}^{\beta}(\mathbf{q})$ . The last line of Eq. (44) contains the source terms, of which the second one gives the contribution by the stimulated emission which is important only if the system is positioned inside a cavity. Hence, we will completely neglect this effect, thus decoupling Eq. (44) from Eq. (42). The source term

$$S_{\beta'}^{\beta}(\mathbf{q}) \equiv \mathcal{F}_{\mathbf{q}} \sum_{\beta_1} (f_{h\beta_1}^{\beta} f_{e\beta'}^{\beta_1} + C_{X\beta_1\beta'}^{\beta_1\beta}) \quad (45)$$

is due to spontaneous emission from either the plasma or correlated electron-hole pairs.

Equations (42) and (44) constitute the *semiconductor luminescence equations* for the quantum dot.

### A. Analytic luminescence formula

In many experimentally relevant situations, the recombination correlations, the densities, and the excitonic correlations are quasistationary quantities. In this case, Eq. (44) leads to

$$(\hbar\omega_{\mathbf{q}} + i\gamma) \Pi_{\beta'}^{\beta}(\mathbf{q}) = \sum_{\beta_1\beta_2} A_{\beta\beta',\beta_1\beta_2} \Pi_{\beta_2}^{\beta_1}(\mathbf{q}) + iS_{\beta'}^{\beta}(\mathbf{q}). \quad (46)$$

This equation has the same structure as the SBE (34) for the microscopic polarization  $p_{\beta'}^{\beta}$ . Hence, we can again diagonalize the problem by means of the exciton basis from Appendix C. We finally obtain

$$I_{\text{PL}}(\omega_{\mathbf{q}}) = \frac{2|\mathcal{F}_{\mathbf{q}}|^2}{\hbar} \text{Im} \left[ \sum_{ij} \frac{\langle \phi^{i,R} | 1 \rangle \langle X_i^{\dagger} X_j \rangle \langle 1 | \phi^{j,R} \rangle}{\mathcal{E}_j - \hbar\omega_{\mathbf{q}} - i\gamma} \right], \quad (47)$$

with the excitonic operators

$$X_i = \sum_{\beta\beta'} (\phi_{\beta\beta'}^{i,L})^* a_{v\beta}^{\dagger} a_{c\beta'}. \quad (48)$$

As in higher-dimensional semiconductor structures, both excitonic correlations (the doublet part  $\Delta \langle X_i^{\dagger} X_j \rangle$ ) and Coulomb-correlated plasma (the singlet part  $\langle X_i^{\dagger} X_j \rangle_{\text{S}}$ ) provide contributions to the spectrum that cannot be distinguished by a standard photoluminescence experiment.<sup>46</sup>

### B. Evolution of spontaneous recombination

In order to close the set of equations, we finally consider the temporal evolution of the source term (45). For the density expectation values in the incoherent regime, the equations of motion (22) and (23) reduce to

$$i\hbar \frac{\partial}{\partial t} f_{e\beta'}^{\beta} = \sum_{\beta_1} (E_{\beta'\beta_1}^e f_{e\beta_1}^{\beta} - E_{\beta_1\beta'}^e f_{e\beta'}^{\beta_1}) - \sum_{\beta_1\beta_2\beta_3} \left[ V_{\beta_2\beta_3}^{\beta'\beta_1} \sum_{\lambda} C \left( \begin{matrix} c\lambda \\ \lambda c \end{matrix} \middle| \begin{matrix} \beta\beta_1 \\ \beta_2\beta_3 \end{matrix} \right) - V_{\beta_2\beta_3}^{\beta\beta_1} \sum_{\lambda} C \left( \begin{matrix} c\lambda \\ \lambda c \end{matrix} \middle| \begin{matrix} \beta_3\beta_2 \\ \beta_1\beta' \end{matrix} \right) \right] + i\Delta \langle B_{\Sigma}^{\dagger} a_{v\beta}^{\dagger} a_{c\beta'} \rangle + i\Delta \langle B_{\Sigma}^{\dagger} a_{v\beta'}^{\dagger} a_{c\beta} \rangle^*, \quad (49)$$

$$i\hbar \frac{\partial}{\partial t} f_{h\beta'}^{\beta} = -\sum_{\beta_1} (E_{\beta'\beta_1}^h f_{h\beta_1}^{\beta} - E_{\beta_1\beta'}^h f_{h\beta'}^{\beta_1}) + \sum_{\beta_1\beta_2\beta_3} \left[ V_{\beta_2\beta_3}^{\beta'\beta_1} \sum_{\lambda} C \left( \begin{matrix} \lambda v \\ v\lambda \end{matrix} \middle| \begin{matrix} \beta_1\beta \\ \beta_3\beta_2 \end{matrix} \right) - V_{\beta_2\beta_3}^{\beta\beta_1} \sum_{\lambda} C \left( \begin{matrix} \lambda v \\ v\lambda \end{matrix} \middle| \begin{matrix} \beta_2\beta_3 \\ \beta'\beta_1 \end{matrix} \right) \right] + i\Delta \langle B_{\Sigma}^{\dagger} a_{v\beta}^{\dagger} a_{c\beta'} \rangle + i\Delta \langle B_{\Sigma}^{\dagger} a_{v\beta'}^{\dagger} a_{c\beta} \rangle^*. \quad (50)$$

For the excitonic correlation (30), we obtain

$$i\hbar \frac{\partial}{\partial t} C_{X\beta''\beta'''}^{\beta\beta'} = -\sum_{\beta_1\beta_2} A_{\beta''\beta,\beta_2\beta_1}^* C_{X\beta_2\beta'''}^{\beta_1\beta'} + \sum_{\beta_1\beta_2} A_{\beta'\beta''',\beta_1\beta_2} C_{X\beta''\beta_2}^{\beta\beta_1} + \sum_{\beta_1\beta_2\beta_3\beta_4} V_{\beta_1\beta_4}^{\beta_2\beta_3} [(\delta_{\beta\beta_1} - f_{e\beta_1}^{\beta})(\delta_{\beta_2\beta'''} - f_{h\beta'''}^{\beta_2}) \times f_{e\beta'''}^{\beta_3} f_{h\beta_4}^{\beta'} - (\delta_{\beta_3\beta'''} - f_{e\beta'''}^{\beta_3})]$$

$$\begin{aligned}
 & \times (\delta_{\beta' \beta_4} - f_{h\beta_4}^{\beta'}) f_{e\beta'}^{\beta} f_{h\beta''}^{\beta_2} \\
 & + D_X^{\text{exc}\beta \beta'} + T_{X\beta''\beta'''}^{\beta \beta'} \\
 & - i(\delta_{\beta\beta''} - f_{h\beta''}^{\beta} - f_{e\beta''}^{\beta}) \Delta \langle B_{\Sigma}^{\dagger} a_{v\beta'}^{\dagger} a_{c\beta''} \rangle \\
 & - i(\delta_{\beta'\beta''} - f_{h\beta''}^{\beta'} - f_{e\beta''}^{\beta'}) \Delta \langle B_{\Sigma}^{\dagger} a_{v\beta''}^{\dagger} a_{c\beta} \rangle^*. \quad (51)
 \end{aligned}$$

Although quite complicated, this equation can be interpreted straightforwardly. The first line would be diagonal in the exciton basis and characterizes  $C_X$  as an “excitonic” correlation. The Coulomb sum beginning in the second line constitutes the source term having the form of a generalized Boltzmann equation. The last two lines are responsible for the radiative decay of the excitonic correlations. Finally,  $D_X^{\text{exc}\beta \beta'}$  denotes all terms originating from the fermionic exchange which are explicitly given in Appendix D. The correlated triplets  $D_{X\beta''\beta'''}^{\beta \beta'}$  are omitted within the pure singlet-doublet analysis performed in this paper.

The equations of motion for the electron-electron and hole-hole correlations have similar structures. Their explicit form can also be found in Appendix D where the relevance of exchange terms and intraband carrier-carrier correlations for the dynamics and optical spectra is briefly discussed.

## VI. NUMERICAL STUDY OF STABLE QUANTUM-DOT STATES

A quantum dot can be excited in several different ways. One possibility involves pumping by means of an optically resonant coherent light field. Other methods include nonresonant optical excitation as well as optical or electronic pumping of the wetting layer where the last two cases imply carrier-capture dynamics between wetting-layer and quantum-dot states.<sup>23</sup> For all indirect excitations, one can anticipate a significant Coulomb and phonon-induced relaxation. To define the form of the excitation, one must, in principle, describe the dynamics of all relevant quantities microscopically. As a simplification, we use in this paper a phenomenological description of the excitation process and restrict the microscopical analysis to the quantum emission from stable dot states in the incoherent regime. For this purpose, we assume a generic form for the pumping of singlets and doublets, demanding that a steady-state configuration is reached after excitation. As additional constraints, the fermionic levels may only be excited to values between 0 and 1, and the steady-state luminescence must be positive. These conditions define the generic phase space of possible excitations.

Explicitly, we model the pumping by adding a term

$$\left. \frac{\partial}{\partial t} \right|_{\text{pump}} Y = Y_0 \dot{S}_Y(t), \quad (52)$$

with  $Y_0$  as the pumping amplitude, to the dynamics of the quantity  $Y$  that can either be a density or a genuine two-particle correlation. Pumping the exciton and plasma densities separately allows us to study the influence of the different population contributions on the emission characteristics.

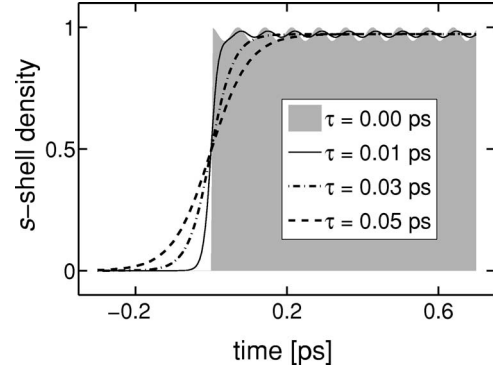


FIG. 4. Pumping of the  $s$ -shell density for different switch-on times  $\tau$ .

The switch-on function  $S_Y(t)$  vanishes in the beginning and approaches unity for large  $t$  while its derivative approaches zero. For all examples throughout this paper, we have chosen a common function

$$S_Y(t) \equiv \frac{1}{1 + e^{-t/\tau}} \quad (53)$$

for all  $Y$ . As long as the the switch-on time  $\tau$  is not too short, the final value of  $Y$  does not depend on  $\tau$ . In order to estimate the shortest admissible  $\tau$ , we consider the simplest case, where only the  $s$ -shell densities  $f_s^{e/h} \equiv f_{e/h(0,0)}^{(0,0)}$  are pumped with amplitude  $Y_0=1$ . The results for four different switch-on times are shown in Fig. 4. Pumping with  $\tau$  larger than 30 fs leads to a well-defined final density while  $\tau = 10$  fs constitutes a too fast switch on such that no stable configuration is reached. As a consequence, all expectation values exhibit periodic oscillations which is most pronounced for an immediate switch on, i.e.,  $\tau \rightarrow 0$ .

Moreover, we observe that for a reasonably slow switch on, the density terminates a little below the value of the pumping amplitude, which expresses the fact that during the excitation, a certain amount of density is transferred to the  $p$  shell. This effect can be traced back to the Coulomb correlations between the shells and is related to the nonvanishing  $\phi_{pp}^{1,R}$  component of the first excitonic wave function (see Fig. 3). Since the comparatively slow radiative decay is the only process in our model that changes the number of carriers per band, the density transfer from  $s$  to  $p$  shell does not change the total density. Because we will exclusively consider situations where electrons and holes are pumped symmetrically, the total number of electron-hole pairs  $N_{eh}$  will be a well-defined quantity in the following.

Next, we analyze how the reached steady state depends on the pumping amplitude. Here, we exclusively treat excitation of the  $s$ -shell density. To be assured that the switch-on process is sufficiently slow in all cases, we choose a large switch-on time  $\tau=270$  fs. As a well-defined way to quantify what kind of excitation is present in the quantum dot, we consider the energy per particle. The total energy of the material system

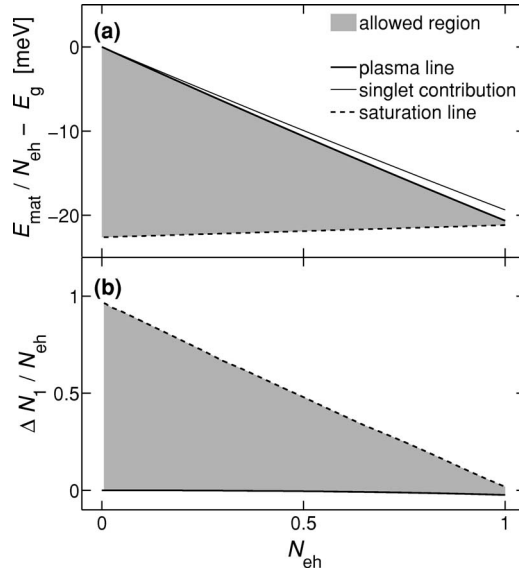


FIG. 5. (a) Total energy  $E_{\text{mat}} = \langle H_{\text{mat}} \rangle$  per particle as function of the total density  $N_{\text{eh}}$  (thick solid line). The thin solid line gives the singlet contribution to the total energy, while the saturation line is defined by the first excitonic resonance. (b) First-exciton population reached for density pumping alone (solid line) and maximum allowed  $\Delta N_1$  pumping (dashed line).

$$\langle H_{\text{mat}} \rangle \equiv \langle H_{0,\text{ele}} \rangle + \langle H_{\text{C}} \rangle \quad (54)$$

decomposes into the singlet contribution

$$\begin{aligned} \langle H_{\text{mat}} \rangle_{\text{S}} = & \sum_{\beta} (E_{\beta}^{\text{e}} f_{\text{e}\beta}^{\beta} - E_{\beta}^{\text{h}} f_{\text{h}\beta}^{\beta}) + \frac{1}{2} \sum_{\beta_1 \dots \beta_4} V_{\beta_3 \beta_4}^{\beta_1 \beta_2} (f_{\text{h}\beta_4}^{\beta_1} f_{\text{h}\beta_3}^{\beta_2} \\ & - f_{\text{h}\beta_3}^{\beta_1} f_{\text{h}\beta_4}^{\beta_2} + f_{\text{e}\beta_4}^{\beta_1} f_{\text{e}\beta_3}^{\beta_2} - f_{\text{e}\beta_3}^{\beta_1} f_{\text{e}\beta_4}^{\beta_2} - 2f_{\text{e}\beta_4}^{\beta_1} f_{\text{h}\beta_3}^{\beta_2}), \end{aligned} \quad (55)$$

where for the Coulomb part, we have taken into account the renormalizations discussed in Sec. IV directly after Eqs. (24) and (25), and the contribution of the two-particle correlations

$$\Delta \langle H_{\text{mat}} \rangle = \frac{1}{2} \sum_{\beta_1 \dots \beta_4} V_{\beta_3 \beta_4}^{\beta_1 \beta_2} (C_{\text{h}\beta_4 \beta_3}^{\beta_1 \beta_2} + C_{\text{e}\beta_4 \beta_3}^{\beta_1 \beta_2} - 2C_{\text{X}\beta_3 \beta_4}^{\beta_1 \beta_2}). \quad (56)$$

Both the total energy (thick solid line) and its singlet contribution (thin solid line), each normalized with respect to the number of excited electron-hole pairs, are plotted in Fig. 5(a) as a function of  $N_{\text{eh}}$ . For low densities, the energy per particle is close to the gap which means that the system is in an electron-hole plasma state where electrons and holes are independent and uncorrelated entities such that the density matrix approximately has the product form  $\rho = \rho_{\text{e}} \otimes \rho_{\text{h}}$ . For elevated densities, however, the total energy per particle approaches the lowest resonance, i.e., the excitonic binding energy  $\mathcal{E}_1$  (dashed line). Moreover, the absolute value of the doublet contribution to the energy per particle becomes larger, indicating that the stable electron-hole states become truly correlated.

In the next step, we additionally allow for pumping of the first exciton population  $\Delta N_1 \equiv \Delta \langle X_1^\dagger X_1 \rangle$ . It turns out that stable excitation states are thus reached for an almost arbitrary pumping amplitude where as a general tendency, the energy per particle decreases with increasing strength of the population pumping. Physically, however, the phenomenological excitation of the lowest exciton population has to be limited such that the total energy per particle does not go below the excitonic binding energy. Hence, the shaded area in Fig. 5(a) designates the physically allowed stable states. From below, it is limited by the excitonic binding energy that defines the *population-saturation line* of the system, and the upper limit is given by the *plasma line* that yields the total energy per particle in the absence of population pumping. Figure 5(b) shows the amount of generated excitonic population per particle for both the saturation regime (solid line) and the plasma regime (dashed line). The shaded area in between indicates the physically allowed phase space for the exciton pumping. We notice that the population per particle assumes values between 0 and 1 and is largest for dilute densities. We conclude that, depending on the excitation conditions, a quantum dot in the low-density regime can have a stable many-body configuration ranging from pure plasma ( $\Delta N/N_{\text{eh}} \approx 0$ ) up to fully correlated electron-hole pairs ( $\Delta N/N_{\text{eh}} \approx 1$ ).

## VII. PHOTOLUMINESCENCE FROM STABLE QUANTUM-DOT STATES

Next, we calculate the luminescence spectra for some exemplary stable states out of the allowed phase space determined in Sec. VI. The justification to concentrate on stable states of the material system is provided by the fact that radiative decay of excitation typically takes place on a comparatively large time scale—radiative lifetimes of less than 1 ns are usually only reached when the spontaneous emission of the dot is drastically enhanced with help of a microcavity<sup>47</sup> or a photonic-crystal environment.<sup>48</sup> We may thus assume that the quantum-dot carrier system remains stationary sufficiently long such that steady-state luminescence can be determined. Under these conditions, the carrier system acts as a constant source for the photoemission.

### A. Low-density regime

The shaded area in Fig. 6(a) displays the luminescence at the first excitonic resonance when the *s*-shell density is weakly pumped with the amplitude 0.1. The dashed and solid curves are obtained by additional pumping of the first exciton. We find that the magnitude of the luminescence increases strongly for higher exciton densities, however, its spectral shape and position are not affected by the population, i.e., luminescence is observed at the excitonic resonance regardless of whether the system is in the plasma or in the population-saturation regime. This behavior can directly be deduced from the explicit form of the steady-state luminescence formula (47) which shows that the emission frequencies are independent of the population source.



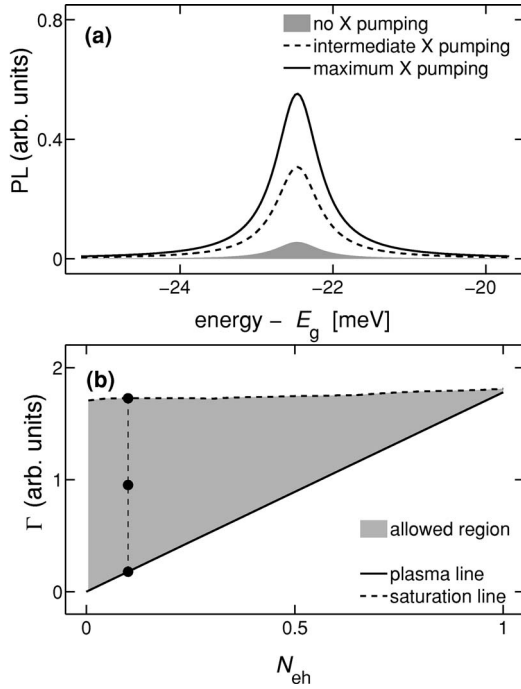


FIG. 6. (a) First luminescence peak in case of weak density pumping for maximum  $\Delta N_1$  pumping (solid line), half-as-strong  $\Delta N_1$  pumping (dashed line), and no  $\Delta N_1$  pumping at all (shaded area). (b) Recombination rate for plasma (solid line) and population-saturation (dashed line) regimes. The bold dots mark the three cases from (a).

From Eq. (42) and Eqs. (49) and (50), it follows that the total number of recombined electron-hole pairs per unit time,

$$-\frac{\partial N_{eh}}{\partial t} = -\frac{\partial}{\partial t} \bigg|_{H_D} \sum_{\beta} f_{e/h\beta}^{\beta} = \frac{2}{\hbar} \frac{\partial}{\partial t} \text{Re} \left[ \sum_{\beta} \Delta \langle B_{\Sigma}^{\dagger} a_{v\beta}^{\dagger} a_{c\beta} \rangle \right] = \frac{\partial}{\partial t} \sum_{\mathbf{q}} \Delta \langle B_{\mathbf{q}}^{\dagger} B_{\mathbf{q}} \rangle, \quad (57)$$

equals the total number of emitted photons per unit time. In Fig. 6(b), the recombination rate

$$\Gamma \equiv -\frac{1}{N_{eh}} \frac{\partial N_{eh}}{\partial t} \quad (58)$$

is plotted for both the plasma and the population-saturation regime. While  $\Gamma$  has a high constant value along the saturation line, it decreases linearly along the plasma line as the density is decreased. Plasma versus exciton luminescence can thus be distinguished by their respective decay dynamics. In general, the system can decay along any curve through the shaded area in Fig. 6(b). The dynamics then allows one to draw conclusions about the nature of the decaying quasistationary states. Microscopically, this is determined by a number of effects such as relaxation, carrier capture, phonon coupling, etc. Only for constant  $\Gamma$  does Eq. (58) describe an exponential decay. However, our analysis indicates that the radiative decay in a quantum dot does not necessarily show an exponential behavior.

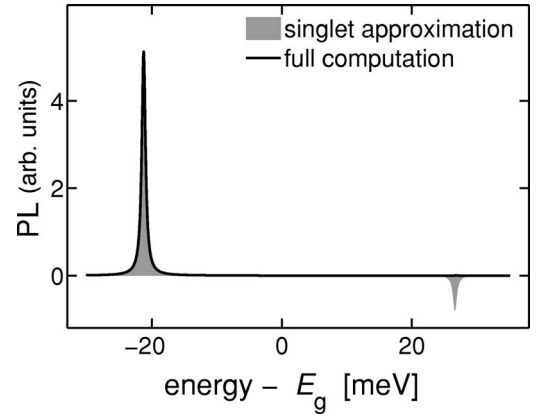


FIG. 7. Luminescence spectrum for a high density of  $N_{eh} = 0.95$ . For the singlet approximation, only the  $f_e f_h$  source term has been considered.

### B. High-density regime

For the luminescence spectrum in Fig. 7, we have pumped the  $s$ -shell density with a high amplitude of 0.95 without any exciton-population pumping. The solid line gives the result of the full computation. We find that even with a high excitation, light is still emitted at the excitonic resonance. While the spectral position of the peak remains almost unchanged compared with the low-density spectrum in Fig. 6, the height of the peak is enlarged by more than one order of magnitude.

The shaded area in Fig. 7 is calculated from the steady-state formula (47) within a singlet approximation where only the  $f_e f_h$  source term from Eq. (45) is considered in the luminescence equation (44). Formally, this corresponds to describing the carrier system by single-particle densities alone, assuming that this would constitute a stable state of the system. This case has already been studied in Fig. 4 with the immediate switch on. From that analysis we see that such a state can actually not be stationary, since the densities are strongly oscillating. Nevertheless, it turns out that the singlet source term alone produces the luminescence at the first resonance rather accurately. On the other hand, an artifact of negative emission is observed at the second excitonic resonance which is a consequence of the instability of the corresponding singlet state. This clearly demonstrates that doublets are necessary to provide a stable state of the system with a physically meaningful steady-state luminescence spectrum. For the given pumping conditions, the singlet approximation underestimates the recombination rate  $\Gamma$  from the full computation by a factor of about 0.74.

### C. Physical relevance of second-exciton pumping

A close inspection of the second excitonic resonance shows that for every  $s$ -shell-pumping amplitude from 0 to 1, one can find a pumping strength of the first exciton such that the luminescence at the second excitonic resonance turns negative. Although for all physically allowed  $\Delta N_1$ -pumping amplitudes the absolute height of the negative peak remains several orders of magnitude smaller than for the artifact from the singlet approximation discussed in Sec. VII B, this would definitely be an unphysical feature of a steady-state lumines-

cence spectrum. To understand the origin of this, we remember the comment to Fig. 4 that pumping of the  $s$ -shell density always affects the  $p$ -shell densities, too. This was traced back to the Coulomb correlations between the shells. In a similar manner, pumping of the first exciton is always accompanied by a change of the population of the second-exciton state. The fact that this influence can lead to negative luminescence is a clear evidence that in certain cases, population of the first exciton without population of the second exciton constitutes an unphysical situation. However, it turns out that this can easily be cured by exciting the second excitonic state very weakly. Within the phase space determined in Fig. 5, the  $\Delta N_2$ -pumping amplitude that is required for luminescence at the second resonance zero is always smaller than  $10^{-3}$ . This additional constraint upon the physically accessible phase space has practically no effect on the emission of light at the first excitonic resonance and on the recombination rate.

### VIII. SUMMARY AND OUTLOOK

In summary, using a cluster-expansion approach we derive SBEs and SLEs for a quantum dot on a wetting layer with parabolic in-plane confinement. We obtain a closed set of equations of motion on the singlet-doublet level. From these, we derive an Elliott formula for the linear absorption spectrum and a steady-state solution for the photoluminescence spectrum. We then investigate the stable carrier configurations for a quantum dot with an  $s$  and a  $p$  shell. On the basis of a general phenomenological description, we obtain rigorous limits for the phase space of physically allowed excitation processes. The theory is evaluated numerically for different stable states of the quantum dot. Stationary luminescence spectra are computed and the excitonic and plasma contributions are identified.

In the future, the theory will be extended to include also higher-order correlation functions with the goal to analyze the quantum statistics of the emission. For example, in order to describe antibunching effects, conditional probabilities of photon detection have to be calculated. In the incoherent regime, these quantities are the truly correlated parts of four-particle expectation values.

### ACKNOWLEDGMENTS

We thank F. Jahnke and co-workers, University Bremen, for discussions on quantum-dot theory. Our research is supported by the Deutsche Forschungsgemeinschaft in the framework of the Quantum Optics in Semiconductors Research Group and by the Optodynamics Center at the Philipps-University, Marburg.

### APPENDIX A: SINGLE-PARTICLE WAVE FUNCTIONS

It has been shown<sup>33</sup> that a lens-shaped quantum dot can accurately be described by a parabolic in-plane confinement potential

$$V_{\text{QD}}^{\kappa}(\rho) = \frac{1}{2} m_{\kappa} \omega_{\kappa}^2 \rho^2, \quad \kappa = e, h, \quad (\text{A1})$$

where  $m_{e/h}$  denotes the effective electron and hole masses, respectively. For the  $z$  confinement perpendicular to the quantum well, we choose

$$V_{\text{QW}}(z) = \begin{cases} 0 & \text{for } |z| \leq \frac{L}{2}, \\ \infty & \text{for } |z| > \frac{L}{2}. \end{cases} \quad (\text{A2})$$

In the envelope-function approximation, the single-particle wave functions then take the form

$$\phi_{\lambda\beta}(\mathbf{r}) = \zeta_{\beta}^{\kappa}(\mathbf{r}) u_{\lambda}(\mathbf{r}) = \varphi_{\beta}^{\kappa}(\rho, \phi) \xi(z) u_{\lambda}(\mathbf{r}), \quad (\text{A3})$$

where  $u_{\lambda}(\mathbf{r}) = u_{\lambda}(\mathbf{k} = \mathbf{0}, \mathbf{r})$  is the Bloch function with band index  $\lambda = v, c$ . The envelope function  $\zeta_{\beta}^{\kappa}(\mathbf{r})$  decomposes into the ground-state wave function for the  $z$  confinement,

$$\xi(z) = \begin{cases} \sqrt{\frac{2}{L}} \cos \frac{\pi}{L} z & \text{for } |z| \leq \frac{L}{2}, \\ 0 & \text{for } |z| > \frac{L}{2}, \end{cases} \quad (\text{A4})$$

and an eigenfunction of the two-dimensional harmonic oscillator in polar coordinates

$$\varphi_{\beta}^{\kappa}(\rho, \phi) = c_0(\beta) e^{im\phi} e^{-\eta\rho^2} \rho^{|m|} L_r^{|m|}(2\eta\rho^2), \quad (\text{A5})$$

where

$$l^{\pm}(\beta) \equiv \frac{1}{2}(n \pm |m|), \quad (\text{A6})$$

$$c_0(\beta) \equiv \frac{1}{\sqrt{\pi}} \sqrt{\frac{l^+!}{l^-!}} (2\eta)^{(1+|m|)/2}, \quad (\text{A7})$$

$$\eta \equiv \frac{m_{\kappa} \omega_{\kappa}}{2\hbar}, \quad (\text{A8})$$

and  $L_r^{|m|}$  denotes the generalized Laguerre polynomial. The corresponding eigenenergies are

$$E_{\beta}^{\text{HO},\kappa} = \hbar \omega_{\kappa} (n + 1). \quad (\text{A9})$$

Neither the eigenenergies nor the eigenstates explicitly depend on the spin. By the choice  $m_e \omega_e = m_h \omega_h$  we obtain identical wave functions for electrons and holes. This characterizes the so-called *symmetric case* which is often employed in the literature.

The second quantization of  $H_{0,\text{ele}}$ ,  $H_C$ , and  $H_D$  from Sec. II has thus been performed with the electronic field operator

$$\Psi(\mathbf{r}) = \sum_{\lambda\beta} a_{\lambda\beta} \phi_{\lambda\beta}(\mathbf{r}), \quad \lambda = v, c. \quad (\text{A10})$$

### APPENDIX B: COULOMB MATRIX ELEMENTS

In second quantization using the field operator (A10), the Coulomb interaction Hamiltonian takes the form

$$H_C = \frac{1}{2} \sum_{\substack{\lambda_1, \dots, \lambda_4 \\ \beta_1, \dots, \beta_4}} a_{\lambda_1 \beta_1}^\dagger a_{\lambda_2 \beta_2}^\dagger a_{\lambda_3 \beta_3} a_{\lambda_4 \beta_4} V \left( \begin{array}{c} \lambda_1 \lambda_2 \\ \lambda_3 \lambda_4 \end{array} \middle| \begin{array}{c} \beta_1 \beta_2 \\ \beta_3 \beta_4 \end{array} \right), \quad (\text{B1})$$

where

$$V \left( \begin{array}{c} \lambda \lambda' \\ \lambda'' \lambda''' \end{array} \middle| \begin{array}{c} \beta \beta' \\ \beta'' \beta''' \end{array} \right) \equiv \int \int d^3 r d^3 r' \phi_{\lambda \beta}^*(\mathbf{r}) \phi_{\lambda' \beta'}^*(\mathbf{r}') V(\mathbf{r} - \mathbf{r}') \phi_{\lambda'' \beta''}(\mathbf{r}') \phi_{\lambda''' \beta'''}(\mathbf{r}) \quad (\text{B2})$$

with the unscreened Coulomb potential

$$V(\mathbf{r} - \mathbf{r}') = \frac{e^2}{4\pi\epsilon_0\epsilon|\mathbf{r} - \mathbf{r}'|}. \quad (\text{B3})$$

To evaluate (B2), we use separation of length scales. We summarize over all unit cells  $\mathbf{R}$  and make use of the periodicity of the Bloch functions  $u_\lambda(\mathbf{r}_0 + \mathbf{R}) = u_\lambda(\mathbf{r}_0)$  and the fact that the envelope function varies slowly in space, such that we can replace  $\zeta_\beta(\mathbf{R} + \mathbf{r}_0)$  by  $\zeta_\beta(\mathbf{R})$  for any unit-cell vector  $\mathbf{r}_0 \in \Omega_0$ . Furthermore, the Bloch functions are orthonormal with respect to the unit cell, and  $\sum_{\mathbf{R}} \Omega_0 f(\mathbf{R}) \simeq \int d^3 R f(\mathbf{R})$ . Finally, we find the matrix elements from Eq. (3) to be

$$V_{\beta_3 \beta_4}^{\beta_1 \beta_2} = \delta_{\sigma_1 \sigma_4} \delta_{\sigma_2 \sigma_3} \int \int d^3 r d^3 r' \zeta_{\beta_1}^*(\mathbf{r}) \zeta_{\beta_2}^*(\mathbf{r}') \times V(\mathbf{r} - \mathbf{r}') \zeta_{\beta_3}(\mathbf{r}') \zeta_{\beta_4}(\mathbf{r}). \quad (\text{B4})$$

For the harmonic-oscillator eigenstates below the dissociation threshold, this volume integral can analytically be reduced to a one-dimensional integral,

$$V_{\beta_3 \beta_4}^{\beta_1 \beta_2} = 2\pi\alpha \delta_{m_1+m_2, m_3+m_4} \delta_{\sigma_1 \sigma_4} \delta_{\sigma_2 \sigma_3} (-1)^{m_3-m_2} \int_0^\infty dq I_0(q) G_{\beta_1 \beta_4}(q) G_{\beta_2 \beta_3}(q), \quad (\text{B5})$$

where we have defined

$$\alpha \equiv \frac{1}{2\sqrt{2}\pi^4} \frac{e^2}{\epsilon_0\epsilon} \sqrt{\frac{m_\kappa \omega_\kappa}{\hbar}}, \quad (\text{B6})$$

$$I_0(q) \equiv \int \int dz dz' |\xi(z)|^2 |\xi(z')|^2 e^{-q\sqrt{\eta}|z-z'|} \quad (\text{B7})$$

and

$$G_{\beta_1 \beta_2}(q) = 2\pi i^{(m_2-m_1)} c_0(\beta_1) c_0(\beta_2) \eta^{-1-(|m_1|+|m_2|)/2} \times \int_0^\infty d\rho \rho e^{-2\rho^2} \rho^{|m_1|+|m_2|} L_{|m_1|}^{m_1}(\rho^2) L_{|m_2|}^{m_2}(\rho^2) \times (2\rho^2) J_{m_2-m_1}(q\rho), \quad (\text{B8})$$

with  $J_m(x)$  the Bessel function of the first kind. The integral (B7) that contains the contribution from the quantum-well confinement can be computed analytically.

### APPENDIX C: EXCITON PROBLEM

The homogeneous part of Eq. (34) defines an  $N^2$ -dimensional eigenvalue problem, where  $N$  is the number of discrete single-particle states per band we have included in our model

$$\mathbf{A}|\phi^{i,R}\rangle = \mathcal{E}_i|\phi^{i,R}\rangle, \quad i = 1, \dots, N^2. \quad (\text{C1})$$

Here,  $|\phi^{i,R}\rangle$  denotes the right-handed excitonic wave function with components  $\phi_{\beta\beta'}^{i,R}$ , while the excitonic eigenenergies  $\mathcal{E}_i$  are the eigenvalues of the  $N^2 \times N^2$  matrix  $\mathbf{A}$  as given by Eq. (35).

It is straightforward to see that the matrix  $\mathbf{A}$  becomes non-Hermitian whenever the densities are nonvanishing. As a consequence, the eigenfunctions  $|\phi^{i,R}\rangle$  do not coincide with the left-handed solutions  $|\phi^{i,L}\rangle$  of the excitonic eigenvalue problem,

$$\langle \phi^{i,L} | \mathbf{A} = \langle \phi^{i,L} | \mathcal{E}_i. \quad (\text{C2})$$

Left- and right-handed eigenfunctions obey the generalized orthonormality and completeness relations

$$\langle \phi^{i,L} | \phi^{j,R} \rangle = \sum_k \langle \phi^{i,L} | k \rangle \langle k | \phi^{j,R} \rangle = \delta_{ij}, \quad (\text{C3})$$

$$\sum_i |\phi^{i,R}\rangle \langle \phi^{i,L}| = \sum_{ijk} |j\rangle \langle j| \phi^{i,R}\rangle \langle \phi^{i,L}| k\rangle \langle k| = \mathbf{1}, \quad (\text{C4})$$

i.e.,  $\{|\phi^{i,R}\rangle\}$  and  $\{|\phi^{i,L}\rangle\}$  are reciprocal.

In view of Eqs. (C3) and (C4), we can introduce excitonic creation and annihilation operators

$$X_i^\dagger \equiv \sum_{\beta\beta'} \phi_{\beta\beta'}^{i,L} a_{c\beta}^\dagger a_{v\beta}, \quad (\text{C5})$$

$$X_i = \sum_{\beta\beta'} (\phi_{\beta\beta'}^{i,L})^* a_{v\beta}^\dagger a_{c\beta'}, \quad (\text{C6})$$

which can be inverted via

$$a_{c\beta'}^\dagger a_{v\beta} = \sum_i (\phi_{\beta\beta'}^{i,R})^* X_i^\dagger, \quad (\text{C7})$$

$$a_{v\beta}^\dagger a_{c\beta'} = \sum_i \phi_{\beta\beta'}^{i,R} X_i \quad (\text{C8})$$

back to the electron-hole picture.

### APPENDIX D: EFFECT OF EXCHANGE TERMS AND INTRABAND CARRIER-CARRIER CORRELATIONS

The exchange terms in the equation of motion (51) for the excitonic correlations explicitly read

$$D_X^{\text{exc}\beta\beta'} = \sum_{\beta_1\beta_2\beta_3\beta_4} V_{\beta_4\beta_2}^{\beta_1\beta_3} [(\delta_{\beta'\beta_2} f_{h\beta'}^{\beta_1} - \delta_{\beta_1\beta'} f_{h\beta_2}^{\beta'}) C_{X-e\beta_4\beta''}^{\beta\beta_3} + (\delta_{\beta_1\beta''} f_{e\beta_2}^{\beta} - \delta_{\beta\beta_2} f_{e\beta''}^{\beta_1}) C_{X-h\beta''\beta_4}^{\beta_3\beta'}] + \sum_{\beta_1\beta_2\beta_3\beta_4} V_{\beta_3\beta_4}^{\beta_1\beta_2} [(\delta_{\beta_2\beta''} f_{h\beta''}^{\beta_1} - \delta_{\beta_1\beta''} f_{e\beta''}^{\beta_2}) C_{X\beta_4\beta_3}^{\beta\beta'}]$$

$$\begin{aligned}
 & + (\delta_{\beta'\beta_1} f_{e\beta_2}^\beta - \delta_{\beta\beta_2} f_{h\beta_1}^{\beta'}) C_{X\beta'\beta''}^{\beta_3\beta_4} \\
 & + \sum_{\beta_1\beta_2\beta_3\beta_4} V_{\beta_2\beta_4}^{\beta_1\beta_3} [(\delta_{\beta_1\beta''} f_{h\beta_2}^{\beta'} - \delta_{\beta'\beta_2} f_{h\beta_1}^{\beta_1}) C_{X\beta_4\beta''}^{\beta\beta_3} \\
 & + (\delta_{\beta\beta_2} f_{e\beta''}^{\beta_1} - \delta_{\beta_1\beta''} f_{e\beta_2}^\beta) C_{X\beta'\beta_4}^{\beta_3\beta'}]. \quad (D1)
 \end{aligned}$$

The first line of Eq. (51) contains two further Coulomb sums over excitonic correlations. There, the density-dependent factors have the phase-space filling form, as can be seen from the definition (35) of the matrix  $\mathbf{A}$ . Hence, for low densities, the structure of the equations of motion for the excitonic correlations is predominantly determined by those Coulomb sums. It is then acceptable to neglect the exchange terms completely, which characterizes the so-called *main-sum approximation*. We have found that even for strong  $s$ -shell pumping the steady-state luminescence spectrum barely changes its shape when this approximation is applied.

In order to ultimately close the set of equations on the singlet-doublet level, we finally need the equations of motion for the intraband carrier-carrier correlations (31) and (32). For the electron-electron correlation (31), we obtain

$$\begin{aligned}
 i\hbar \frac{\partial}{\partial t} C_{e\beta'\beta''}^{\beta\beta'} & = \sum_{\beta_1} (E_{\beta_1\beta}^e C_{e\beta'\beta''}^{\beta_1\beta'} + E_{\beta_1\beta'}^e C_{e\beta''\beta_1}^{\beta\beta_1} - E_{\beta''\beta_1}^e C_{e\beta_1\beta''}^{\beta\beta'}) \\
 & - E_{\beta''\beta_1}^e C_{e\beta'\beta_1}^{\beta\beta'} + \sum_{\beta_1\beta_2\beta_3\beta_4} (V_{\beta_4\beta_3}^{\beta_1\beta_2} - V_{\beta_3\beta_4}^{\beta_1\beta_2}) \\
 & \times [f_{e\beta_1}^\beta f_{e\beta_2}^{\beta'} (\delta_{\beta_3\beta''} - f_{e\beta''}^{\beta_3}) (\delta_{\beta_4\beta''} - f_{e\beta''}^{\beta_4}) \\
 & - f_{e\beta''}^{\beta_3} f_{e\beta_2}^{\beta_4} (\delta_{\beta\beta_1} - f_{e\beta_1}^\beta) (\delta_{\beta'\beta_2} - f_{e\beta_2}^{\beta'})] \\
 & + \sum_{\beta_1\beta_2\beta_3\beta_4} V_{\beta_4\beta_2}^{\beta_1\beta_3} [(\delta_{\beta_1\beta''} f_{e\beta_2}^{\beta'} - \delta_{\beta'\beta_2} f_{e\beta''}^{\beta_1}) C_{X-e\beta_4\beta''}^{\beta\beta_3} \\
 & + (\delta_{\beta_1\beta''} f_{e\beta_2}^\beta - \delta_{\beta\beta_2} f_{e\beta''}^{\beta_1}) C_{X-e\beta_4\beta''}^{\beta'\beta_3} - (\delta_{\beta_1\beta''} f_{e\beta_2}^{\beta'} \\
 & - \delta_{\beta'\beta_2} f_{e\beta''}^{\beta_1}) C_{X-e\beta_4\beta''}^{\beta\beta_3} - (\delta_{\beta_1\beta''} f_{e\beta_2}^\beta \\
 & - \delta_{\beta\beta_2} f_{e\beta''}^{\beta_1}) C_{X-e\beta_4\beta''}^{\beta'\beta_3}] \\
 & + \sum_{\beta_1\beta_2\beta_3\beta_4} V_{\beta_4\beta_3}^{\beta_1\beta_2} [(\delta_{\beta\beta_1} \delta_{\beta'\beta_2} - \delta_{\beta'\beta_2} f_{e\beta_1}^\beta \\
 & - \delta_{\beta\beta_1} f_{e\beta_2}^{\beta'}) C_{e\beta''\beta_4}^{\beta_3\beta_4} - (\delta_{\beta_1\beta''} \delta_{\beta_2\beta''} - \delta_{\beta_1\beta''} f_{h\beta_2}^{\beta_2} \\
 & - \delta_{\beta_2\beta''} f_{h\beta_1}^{\beta_1}) C_{e\beta_4\beta_3}^{\beta\beta'}] - \sum_{\beta_1\beta_2\beta_3\beta_4} V_{\beta_2\beta_4}^{\beta_1\beta_3} [(\delta_{\beta_1\beta''} f_{e\beta_2}^{\beta'} \\
 & - \delta_{\beta'\beta_2} f_{e\beta''}^{\beta_1}) C_{e\beta''\beta_4}^{\beta\beta_3} + (\delta_{\beta_1\beta''} f_{e\beta_2}^\beta \\
 & - \delta_{\beta\beta_2} f_{e\beta''}^{\beta_1}) C_{e\beta_4\beta_3}^{\beta_3\beta'} + (\delta_{\beta_1\beta''} f_{e\beta_2}^{\beta'} \\
 & - \delta_{\beta'\beta_2} f_{e\beta''}^{\beta_1}) C_{e\beta_4\beta_3}^{\beta\beta_3} + (\delta_{\beta_1\beta''} f_{e\beta_2}^\beta \\
 & - \delta_{\beta\beta_2} f_{e\beta''}^{\beta_1}) C_{e\beta_4\beta_3}^{\beta_3\beta'} + (\delta_{\beta_1\beta''} f_{e\beta_2}^{\beta'} \\
 & - \delta_{\beta'\beta_2} f_{e\beta''}^{\beta_1}) C_{e\beta_4\beta_3}^{\beta\beta_3}]. \quad (D2)
 \end{aligned}$$

and for the hole-hole correlation (32)

$$\begin{aligned}
 i\hbar \frac{\partial}{\partial t} C_{h\beta''\beta'''}^{\beta\beta'} & = \sum_{\beta_1} (-E_{\beta_1\beta}^h C_{h\beta''\beta'''}^{\beta_1\beta'} - E_{\beta_1\beta'}^h C_{h\beta''\beta'''}^{\beta\beta_1} + E_{\beta''\beta_1}^h C_{h\beta_1\beta'''}^{\beta\beta'}) \\
 & + E_{\beta''\beta_1}^h C_{h\beta''\beta_1}^{\beta\beta'}) + \sum_{\beta_1\beta_2\beta_3\beta_4} (V_{\beta_4\beta_3}^{\beta_1\beta_2} - V_{\beta_3\beta_4}^{\beta_1\beta_2}) [(\delta_{\beta\beta_1} \\
 & - f_{h\beta_1}^\beta) (\delta_{\beta'\beta_2} - f_{h\beta_2}^{\beta'}) f_{h\beta''\beta'''}^{\beta_3\beta_4} - (\delta_{\beta_3\beta''} - f_{h\beta''}^{\beta_3}) \\
 & \times (\delta_{\beta_4\beta''} - f_{h\beta''}^{\beta_4}) f_{h\beta_1\beta_2}^{\beta'}] \\
 & + \sum_{\beta_1\beta_2\beta_3\beta_4} V_{\beta_4\beta_2}^{\beta_1\beta_3} [(\delta_{\beta'\beta_2} f_{h\beta_2}^{\beta_1} \\
 & - \delta_{\beta_1\beta''} f_{h\beta_2}^{\beta'}) C_{X-h\beta''\beta_4}^{\beta_3\beta} + (\delta_{\beta\beta_2} f_{h\beta_2}^{\beta_1} \\
 & - \delta_{\beta_1\beta''} f_{h\beta_2}^\beta) C_{X-h\beta''\beta_4}^{\beta_3\beta'} - (\delta_{\beta'\beta_2} f_{h\beta_2}^{\beta_1} \\
 & - \delta_{\beta_1\beta''} f_{h\beta_2}^{\beta'}) C_{X-h\beta''\beta_4}^{\beta_3\beta} - (\delta_{\beta\beta_2} f_{h\beta_2}^{\beta_1} \\
 & - \delta_{\beta_1\beta''} f_{h\beta_2}^\beta) C_{X-h\beta''\beta_4}^{\beta_3\beta'}] \\
 & - \sum_{\beta_1\beta_2\beta_3\beta_4} V_{\beta_4\beta_3}^{\beta_1\beta_2} [(\delta_{\beta\beta_1} \delta_{\beta'\beta_2} - \delta_{\beta'\beta_2} f_{h\beta_1}^\beta \\
 & - \delta_{\beta\beta_1} f_{h\beta_2}^{\beta'}) C_{h\beta''\beta'''}^{\beta_3\beta_4} - (\delta_{\beta_1\beta''} \delta_{\beta_2\beta''} - \delta_{\beta_1\beta''} f_{h\beta_2}^{\beta_2} \\
 & - \delta_{\beta_2\beta''} f_{h\beta_1}^{\beta_1}) C_{h\beta_4\beta_3}^{\beta\beta'}] + \sum_{\beta_1\beta_2\beta_3\beta_4} V_{\beta_2\beta_4}^{\beta_1\beta_3} [(\delta_{\beta_1\beta''} f_{h\beta_2}^{\beta'} \\
 & - \delta_{\beta'\beta_2} f_{h\beta''}^{\beta_1}) C_{h\beta''\beta_4}^{\beta\beta_3} + (\delta_{\beta_1\beta''} f_{h\beta_2}^\beta \\
 & - \delta_{\beta\beta_2} f_{h\beta''}^{\beta_1}) C_{h\beta_4\beta_3}^{\beta_3\beta'} + (\delta_{\beta_1\beta''} f_{h\beta_2}^{\beta'} \\
 & - \delta_{\beta'\beta_2} f_{h\beta''}^{\beta_1}) C_{h\beta_4\beta_3}^{\beta\beta_3} + (\delta_{\beta_1\beta''} f_{h\beta_2}^\beta \\
 & - \delta_{\beta\beta_2} f_{h\beta''}^{\beta_1}) C_{h\beta_4\beta_3}^{\beta_3\beta'} + (\delta_{\beta_1\beta''} f_{h\beta_2}^{\beta'} \\
 & - \delta_{\beta'\beta_2} f_{h\beta''}^{\beta_1}) C_{h\beta_4\beta_3}^{\beta\beta_3}]. \quad (D3)
 \end{aligned}$$

Aside from the fact that the electron-electron and hole-hole correlations do not directly couple to the light field, the latter two equations have a very similar structure to the equation of motion for the excitonic correlation. The full numerical calculations show that the intraband correlations only yield very small corrections to the density and exciton-correlation dynamics that naturally become slightly more important when the carrier density increases. The effect of these corrections on the luminescence spectra is even less significant than the effect of the exchange terms (D1).

\*Electronic address: thomas.feldtmann@physik.uni-marburg.de

<sup>1</sup>P. Michler, A. Imamoglu, M. D. Mason, P. J. Carson, G. F. Strouse, and S. K. Buratto, *Nature (London)* **406**, 968 (2000).

<sup>2</sup>P. Michler, A. Kiraz, C. Becher, W. V. Schoenfeld, P. M. Petroff,

L. Zhang, E. Hu, and A. Imamoglu, *Science* **290**, 2282 (2000).

<sup>3</sup>E. Dekel, D. Regelman, D. Gershoni, E. Ehrenfreund, W. V. Schoenfeld, and P. M. Petroff, *Phys. Rev. B* **62**, 11038 (2000).

<sup>4</sup>C. Santori, M. Pelton, G. Solomon, Y. Dale, and Y. Yamamoto,



- Phys. Rev. Lett. **86**, 1502 (2001).
- <sup>5</sup>C. Becher, A. Kiraz, P. Michler, A. Imamoglu, W. V. Schoenfeld, P. M. Petroff, L. Zhang, and E. Hu, Phys. Rev. B **63**, 121312(R) (2001).
- <sup>6</sup>E. Moreau, I. Robert, L. Manin, V. Thierry-Mieg, J. M. Gerard, and I. Abram, Phys. Rev. Lett. **87**, 183601 (2001).
- <sup>7</sup>C. H. Bennett and G. Brassard in *Proceedings of the IEEE International Conference on Computers, Systems, and Signal Processing, Bangalore, India, 1984* (IEEE, New York, 1984), p. 175.
- <sup>8</sup>D. Loss and D. P. DiVincenzo, Phys. Rev. A **57**, 120 (1998).
- <sup>9</sup>F. Troiani, U. Hohenester, and E. Molinari, Phys. Status Solidi B **224**, 849 (2001).
- <sup>10</sup>E. Beham, M. Betz, S. Trumm, M. Kroutvar, Y. Ducommun, H. J. Krenner, M. Bichler, A. Leitenstorfer, J. J. Finley, A. Zrenner, and G. Abstreiter, Phys. Status Solidi C **1**, 2131 (2004).
- <sup>11</sup>Y. Z. Hu, M. Lindberg, and S. W. Koch, Phys. Rev. B **42**, 1713 (1990).
- <sup>12</sup>A. Barenco and M. A. Dupertuis, Phys. Rev. B **52**, 2766 (1995).
- <sup>13</sup>Y. Z. Hu, H. Gießen, N. Peyghambarian, and S. W. Koch, Phys. Rev. B **53**, 4814 (1996).
- <sup>14</sup>A. Wojs and P. Hawrylak, Phys. Rev. B **55**, 13066 (1997).
- <sup>15</sup>P. Hawrylak, Phys. Rev. B **60**, 5597 (1999).
- <sup>16</sup>E. Dekel, D. Gershoni, E. Ehrenfreund, J. M. Garcia, and P. M. Petroff, Phys. Rev. B **61**, 11009 (2000).
- <sup>17</sup>U. Hohenester and E. Molinari, Phys. Status Solidi B **221**, 19 (2000).
- <sup>18</sup>N. Baer, P. Gartner, and F. Jahnke, Eur. Phys. J. B **42**, 231 (2004).
- <sup>19</sup>M. Braskén, M. Lindberg, D. Sundholm, and J. Olsen, Phys. Rev. B **64**, 035312 (2001).
- <sup>20</sup>S. Corni, M. Braskén, M. Lindberg, J. Olsen, and D. Sundholm, Phys. Rev. B **67**, 045313 (2003).
- <sup>21</sup>S. Corni, M. Braskén, M. Lindberg, J. Olsen, and D. Sundholm, Phys. Rev. B **67**, 085314 (2003).
- <sup>22</sup>For reviews and references, see L. Banyai and S. W. Koch, *Semiconductor Quantum Dots* (World Scientific, Singapore, 1993); U. Woggon, *Optical Properties of Semiconductor Quantum Dots* (Springer-Verlag, Berlin, 1996); L. Jacak, P. Hawrylak, and A. Wojs, *Quantum Dots* (Springer-Verlag, Berlin, 1998).
- <sup>23</sup>T. R. Nielsen, P. Gartner, and F. Jahnke, Phys. Rev. B **69**, 235314 (2004), and references therein.
- <sup>24</sup>P. Borri, W. Langbein, U. Woggon, V. Stavarache, D. Reuter, and A. D. Wieck, Phys. Rev. B **71**, 115328 (2005), and references therein.
- <sup>25</sup>J. Fricke, Ann. Phys. (N.Y.) **252**, 479 (1996).
- <sup>26</sup>M. Kira and S. W. Koch, Eur. Phys. J. D **36**, 143 (2005), and references therein.
- <sup>27</sup>M. Kira and S. W. Koch, Phys. Rev. A **73**, 013813 (2006).
- <sup>28</sup>M. Lindberg and S. W. Koch, Phys. Rev. B **38**, 3342 (1988).
- <sup>29</sup>C. Cohen-Tannoudji, J. Dupont-Roc, and G. Grynberg, *Photons and Atoms* (Wiley Interscience, New York, 1989).
- <sup>30</sup>M. Kira, F. Jahnke, W. Hoyer, and S. W. Koch, Prog. Quantum Electron. **23**, 189 (1999).
- <sup>31</sup>G. Bastard, *Wave Mechanics Applied to Semiconductor Heterostructures* (Les Editions de Physique, Paris, 1988).
- <sup>32</sup>H. Haug and S. W. Koch, *Quantum Theory of the Optical and Electronic Properties of Semiconductors*, 4th ed. (World Scientific, Singapore, 2004).
- <sup>33</sup>A. Wojs, P. Hawrylak, S. Fafard, and L. Jacak, Phys. Rev. B **54**, 5604 (1996).
- <sup>34</sup>W. Schäfer and M. Wegener, *Semiconductor Optics and Transport Phenomena* (Springer-Verlag, Berlin, 2002).
- <sup>35</sup>F. E. Harris, H. J. Monkhorst, and D. L. Freeman, *Algebraic and Diagrammatic Methods in Many-Fermion Theory* (Oxford University Press, New York, 1992).
- <sup>36</sup>H. W. Wyld and B. D. Fried, Ann. Phys. (N.Y.) **23**, 374 (1963).
- <sup>37</sup>M. Kira, W. Hoyer, T. Stroucken, and S. W. Koch, Phys. Rev. Lett. **87**, 176401 (2001).
- <sup>38</sup>W. Hoyer, M. Kira, and S. W. Koch, Phys. Rev. B **67**, 155113 (2003).
- <sup>39</sup>H. C. Schneider, W. W. Chow, and S. W. Koch, Phys. Rev. B **64**, 115315 (2001).
- <sup>40</sup>H. C. Schneider, W. W. Chow, and S. W. Koch, Phys. Rev. B **66**, 041310(R) (2002).
- <sup>41</sup>H. C. Schneider, W. W. Chow, and S. W. Koch, Phys. Rev. B **70**, 235308 (2004).
- <sup>42</sup>R. Elliott, in *Polarons and Excitons*, edited by C. Kuper and G. Whitefield (Oliver and Boyd Boston, 1963), p. 269.
- <sup>43</sup>F. Jahnke, M. Kira, S. W. Koch, G. Khitrova, E. K. Lindmark, T. R. Nelson, Jr., D. V. Wick, J. D. Berger, O. Lyngnes, H. M. Gibbs, and K. Tai, Phys. Rev. Lett. **77**, 5257 (1996).
- <sup>44</sup>S. Chatterjee, C. Ell, S. Mosor, G. Khitrova, H. M. Gibbs, W. Hoyer, M. Kira, S. W. Koch, J. P. Prineas, and H. Stolz, Phys. Rev. Lett. **92**, 067402 (2004).
- <sup>45</sup>S. W. Koch, M. Kira, W. Hoyer, and V. Filipinov, Phys. Status Solidi B **238**, 404 (2003).
- <sup>46</sup>M. Kira, F. Jahnke, and S. W. Koch, Phys. Rev. Lett. **81**, 3263 (1998).
- <sup>47</sup>G. S. Solomon, M. Pelton, and Y. Yamamoto, Phys. Rev. Lett. **86**, 3903 (2001).
- <sup>48</sup>P. Lodahl, A. F. van Driel, I. S. Nikolaev, A. Irman, K. Overgaag, D. Vanmaekelbergh, and W. L. Vos, Nature (London) **430**, 654 (2004).